Atmospheric Research 334 (2026) 108774

Contents lists available at ScienceDirect

Atmospheric Research

journal homepage: www.elsevier.com/locate/atmosres

Cost-benefit analysis of the nesting approach in HARMONIE-AROME for a supercell outbreak case study

J. Díaz-Fernández [a,b,*], C. Calvo-Sancho [c], M. López-Reyes [d,e], P. Bolgiani [d], J.J. González-Alemán [b], A. Morata [b], D. Santos-Muñoz [e,f], M.L. Martín [a,g,*]

[a] Department of Applied Mathematics, Faculty of Computer Engineering, University of Valladolid, Segovia, Spain
[b] State Meteorological Agency (AEMET), Madrid, Spain
[c] Centro de Investigaciones sobre Desertificación, Consejo Superior de Investigaciones Científicas (CIDE, CSIC-UV-GVA), Climate, Atmosphere and Ocean Laboratory (Climatoc-Lab), Moncada, Valencia, Spain
[d] Department of Earth Physics and Astrophysics, Faculty of Physics, Complutense University of Madrid, Madrid, Spain
[e] Instituto de Astronomía y Meteorología (IAM), Departamento de Física, Centro Universitario de Ciencias Exactas e Ingenierías, Universidad de Guadalajara, Guadalajara, Mexico
[f] Danmarks Meteorologiske Institut, Copenhagen, Denmark
[g] Institute of Interdisciplinary Mathematics (IMI), Complutense University of Madrid, Madrid, Spain

ARTICLE INFO

Keywords:
Convection
HARMONIE-AROME
Nesting approach
Supercells
Verification

ABSTRACT

Supercells are among the most hazardous convective systems, frequently producing large hail, destructive winds, and severe socio-economic impacts. The enhancement of weather simulations is identified as a primary strategy to optimise short-term forecasting. The present study investigates the performance of two high-resolution configurations of the HARMONIE-AROME model during a severe supercell outbreak over eastern Iberia on 31st July 2015, when six confirmed supercells caused significant damage. The setups tested include a two-step one-way nested approach (2.5 km outer domain and 500 m inner domain), and a single-domain configuration at 500 m resolution. The model outputs, which include reflectivity, precipitation and temperature, are validated against OPERA radar composites and surface observations. At the same time, key convective parameters, derived from the Murcia sounding, are analyzed to assess the pre-convective environment. Although the simulations demonstrate a similar structure to the observed event, the two-domain nested simulation offers a slightly superior depiction of reflectivity and thermodynamic profiles. Nevertheless, precipitation analysis reveals that while nesting improves moderate rainfall representation, it introduces larger errors for the most extreme amounts, limiting its overall benefit. The obtained gain is not sufficient to offset the 30% higher computational cost when the two-domain nested approach is used. The single-domain non-nested configuration demonstrates a superior level of efficiency, exhibiting equivalent accuracy while exhibiting a diminished resource requirement.

1. Introduction

Supercells are the most severe and organized deep convective storm cells in the mesoscale, characterized by the presence of a deep, persistent mesocyclone (Browning, 1962). These thunderstorms are associated with severe weather phenomena, such as lightning, large hail, strong winds, tornadoes or flash floods, which can result in significant property damage, injuries and fatalities (Dahl, 2006; Duda and Gallus, 2010; Kunz et al., 2020; Martín et al., 2021; Nisi et al., 2016; Quirantes Calvo et al., 2014). Deep moist convection and hail formation are typically associated with lower-tropospheric moisture, atmospheric instability, and wind shear (Davies and Johns, 2011; Gascón et al., 2015; Markowski and Richardson, 2010). Large hail in Europe is usually observed in environments characterized by high boundary layer moisture, elevated lifting condensation levels, and high Convective Available Potential Energy (CAPE) (Calvo-Sancho et al., 2022; Kaltenböck et al., 2009; Púčik et al., 2015; Taszarek et al., 2017). Additionally, large-scale atmospheric patterns, such as deep troughs at 500 hPa and baroclinic short waves, have been identified as key contributors to hail formation (García-Ortega et al., 2014; Mora et al., 2015).

Accurately forecasting supercells and their associated hazards is essential for anticipating their impacts and issuing timely warnings.

* Corresponding authors at: Department of Applied Mathematics, Faculty of Computer Engineering, University of Valladolid, Segovia, Spain.
E-mail address: mlmartin@uva.es (M.L. Martín).

https://doi.org/10.1016/j.atmosres.2026.108774
Received 17 November 2025; Received in revised form 9 January 2026; Accepted 12 January 2026
Available online 13 January 2026

Reanalysis products have been widely used to study severe convective storms across Europe (Púcik et al., 2019; Rodríguez and Bech, 2021; Taszarek, 2020; Westermayer et al., 2017) and, more specifically, supercells in Spain (Calvo-Sancho et al., 2022; Calvo-Sancho and Martín, 2021; Rigo et al., 2022). Complementing these reanalysis, dynamical downscaling with convection-permitting Numerical Weather Prediction (NWP) models provides a more detailed representation of atmospheric environments. High-resolution simulations have been applied to study synoptic and mesoscale conditions in tornado events in Italy (Avolio and Miglietta, 2021), convective storms over the Czech Republic (Bližňák et al., 2017), hailstorms in Switzerland (Trefalt et al., 2018) and Southwestern Europe (Merino et al., 2013), as well as idealized supercell dynamics (Markowski and Dotzek, 2011). Moreover, recent studies in the Mediterranean basin have highlighted the complexity of supercell dynamics and their associated hazards. The analysis of development of tornadoes in the Po Valley (De Martin et al., 2024) or the occurrence of giant hail in the Adriatic Sea (Tiesi et al., 2022) underscore the need for high-resolution modelling to capture local scale interactions.

The nesting approach in limited-area models involves embedding a high-resolution domain within a coarser-resolution domain. The outer, coarser domain provides boundary and initial conditions for the inner, finer domain, allowing the simulation of small-scale processes. This method provides enhanced spatial and temporal resolution, flexibility, and region-specific parametrizations, which are essential for accurate simulation of local phenomena. However, challenges can include error propagation from the coarser to the finer domain and high computational cost (De Elía et al., 2002). In this study, two different nested strategies of the HIRLAM-ALADIN Research on Mesoscale Operational Numerical weather prediction in Euromed-Applications of Research to Operations at Mesoscale model (HARMONIE-AROME) are used to assess their performance in simulating reflectivity, precipitation and temperature during a severe convective event. The reflectivity of NWPs has been widely used by several authors (Park et al., 2019; Pilguj et al., 2019) to investigate severe convective weather events and to compare simulations with the Operational Program for Exchange of Weather Radar Information (OPERA).

This study presents a novel cost-benefit analysis of two HARMONIE-AROME configurations—one nested and one single-domain—applied to a severe supercell outbreak on 31 July 2015 that produced severe convective phenomena over complex terrain due to at least six reported supercells in eastern Iberia. This event was selected because it provides an ideal benchmark for testing the added value of high-resolution nested configurations under conditions where accurate representation of mesoscale and convective-scale processes is critical. While the use of a single event limits the generalization of the results, the analysis serves as proof of concept. This evaluation is conducted using the High-Performance Computing Facilities (HPCF) of European Centre for Medium-Range Weather Forecasts (ECMWF), which is in practical terms the only platform where the HARMONIE-AROME model can be executed due to its closed-source nature and licensing restrictions, and the best fitted computer as it was built ad hoc to run this model. Therefore, the main objective of this paper is to assess the HARMONIE-AROME behaviour when nesting is used in comparison of using a single-domain configuration for that supercell, evaluating the cost-benefit tradeoff of the nesting strategy within the ECMWF HPCF environment. To our knowledge, this is the first such evaluation for this model, providing practical insights into future operational and research applications.

This paper is organized as follows: the experimental design, methodology, the NWP model set-up and the observational data are presented in Section 2. Section 3 contains the main results of the validation, while Section 4 has the summary and overall conclusions.

2. Experimental design and methodology

2.1. Dataset and synoptic configuration

The supercell sample used here was selected from the Spanish Supercell Database (Martín et al., 2021), which spans the period 2011–2022 and includes a total of 286 confirmed supercells observations. This dataset comprises all documented supercell events in Spain, with confirmation based on Doppler radar imagery, reports of hail exceeding 5 cm in diameter, tornadoes rated EF2 or higher, or graphical evidence of the event. From this database, July 31, 2015, was chosen for analysis as it represents the day with the highest number of confirmed supercell occurrences. On this date, six supercells were observed over eastern Iberia (Fig. 1a), four of which produced large hail (diameter >5 cm; Table 1).

Eastern Iberia is characterized by a complex orography, including several mountain ranges and valleys —such as the Pyrenees, the Ebro Valley, and the Iberian System, with elevations ranging from 600 m to 2000 m (Fig. 1b) — which contribute to the development of severe weather (Castro et al., 1992; García-Ortega et al., 2014; Merino et al., 2013). In fact, many of the supercell events recorded in the Spanish Supercell Database have occurred within this region (Calvo-Sancho et al., 2022; Martín et al., 2021). Furthermore, the frequency of thunderstorms in this area peaks during the summer months, coinciding with maximum insolation (Calvo-Sancho et al., 2022; Kotroni and Lagouvardos, 2016; Taszarek et al., 2018).

The synoptic setup favoured the development of six supercells over the eastern Iberian Peninsula on 31 July 2015 at 12:00 UTC. At mid-levels, the 500-hPa geopotential height field (Fig. 2a) displays a deep shortwave trough across the region, favoring large-scale vertical motions and instability. This trough is associated with a strong geopotential height gradient, enhancing baroclinicity and promoting deep convection (Mora et al., 2015; Calvo-Sancho et al., 2022). Additionally, the eastern Iberia Peninsula is located in the left-exit of the jet streak, where positive vorticity advection and upper-level divergence further strengthen synoptic forcing (Markowski and Richardson, 2010; Mora et al., 2015; Calvo-Sancho et al., 2022). At the surface, a thermal low-pressure system over central Iberia (Font, 2000) promotes moisture convergence and enhances lifting mechanisms, facilitating convective storm initiation (De Martin et al., 2025; Homar et al., 2003; Miglietta et al., 2017; Taszarek et al., 2019).

The 2-m dewpoint field (Fig. 2b) reveals a strong moisture gradient, with values exceeding 20 °C along the Mediterranean coast, indicative of substantial low-level moisture availability, enhancing instability and providing energy for supercells. This aligns with studies like Romero et al. (2000), which identified moisture pooling along the Mediterranean as a key factor for convective activity in Spain. The associated wind field at 10 m displays a well-defined southerly flow advecting warm and moist air inland, showing convergent airflow towards the eastern Iberian Peninsula. This convergence enhances upward motion and can serve as a trigger for convective initiation (Romero et al., 2000). Moreover, wind shear can be inferred in the area of interest, with southwest winds at low levels and west winds at mid-levels (Rotunno and Klemp, 1982).

These results align with previous research on supercell environments in Spain. Calvo-Sancho et al. (2022) reported a higher frequency of supercells along the Mediterranean coast during the warm season, while Farnell Barqué et al. (2024) highlighted the importance of mesoscale features, such as localized moisture pooling and thermal gradients, in enhancing supercell potential during a hailstorm event in Catalonia, Spain.

2.2. NWP Model set-up

July 31, 2015, supercell outbreak was simulated using ECMWF high-performance computing facilities HPCF with two different nesting

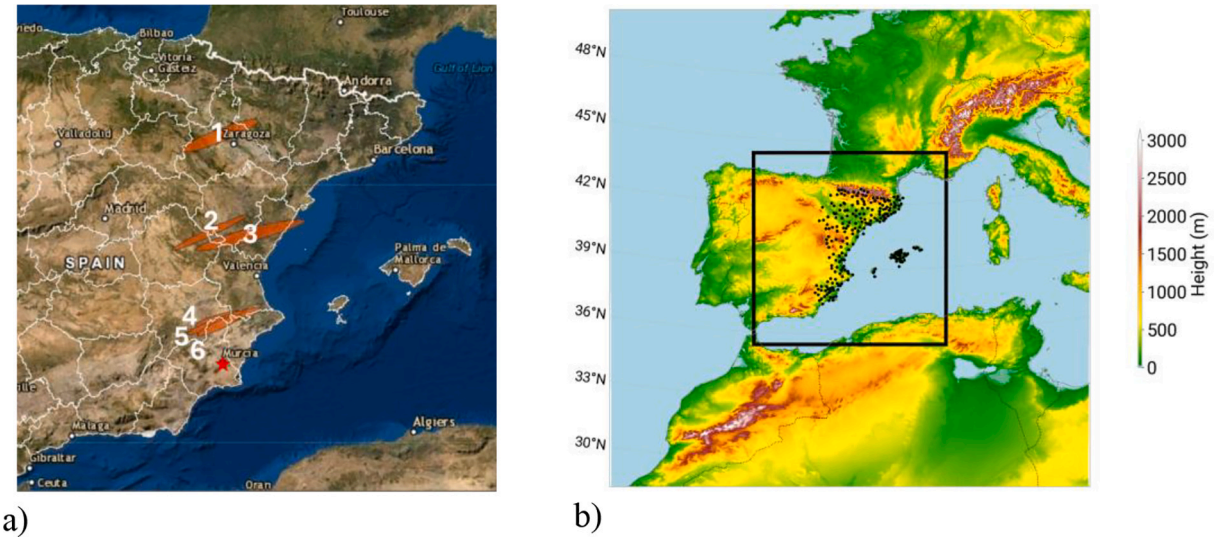

Fig. 1. a) Ellipse tracks for the six supercells reported on July 31, 2015, from the Spanish Supercell Database. Red star indicates the location of Murcia sounding station. b) Orography of the study area and HARMONIE-AROME domain configuration. Outer boundary corresponds to 2.5 km horizontal resolution used in H500_NESTED and the black rectangle indicates 500-m horizontal resolution from H500_NESTED and H500 simulations. Weather stations are denoted by black points. (For interpretation of the references to colour in this figure legend, the reader is referred to the web version of this article.)

Table 1
Supercell events reported from the Spanish Supercell Database on July 31, 2015, with the initial and end time, location and hail size. No hail can refer to hail less than 5 cm in diameter or not reported hail.

ID	Initial time (UTC)	End time (UTC)	Lat	Lon	Hail
SP-1	10:20	13:10	41.77°	−1.18°	6 cm
SP-2	12:10	15:30	40.18°	−1.40°	No
SP-3	13:40	17:20	40.14°	−0.52°	8 cm
SP-4	14:30	16:00	38.69°	−1.10°	5 cm
SP-5	14:50	17:10	38.72°	−1.22°	8 cm
SP-6	18:50	20:50	38.62°	−1.19°	No

strategies of the high-resolution HARMONIE-AROME model (cycle 46 h1) to evaluate and compare their performance (Bengtsson et al., 2017). HARMONIE-AROME is a non-hydrostatic model based on spectral dynamics; thus, the prognosis and process of variables differ fundamentally from models like WRF that use finite-difference methods. This spectral formulation allows for efficient and accurate representation of atmospheric processes at high resolution. The HARMONIE-AROME model has been successfully applied in previous studies focusing on severe convective phenomena, including tropical transition events (Calvo-Sancho et al., 2023a, 2023b; Quitián-Hernández et al., 2021). The first simulation, i.e. H500_NESTED, was run using a two-step one-way dynamic nesting approach, in which a parent (outer) domain with a 2.5 km horizontal resolution provides initial and boundary conditions for a higher-resolution 500 m nested domain (Fig. 1b). This configuration applies dynamic downscaling through a one-way nesting approach, in which the nested high-resolution domain inherits atmospheric conditions from the coarser parent domain without providing feedback. This method has been widely implemented and validated in other limited-area models (Skamarock et al., 2021), and is adapted here for use with the HARMONIE-AROME model. The one-way nesting ensures consistency with large-scale synoptic conditions while allowing for a more detailed and realistic representation of local mesoscale processes (Giorgi and Mearns, 1999). In contrast, the second simulation, i.e. H500, was performed using a single-domain configuration with a uniform 500 m horizontal resolution, providing a direct high-resolution representation of the event without nesting. By comparing these two approaches, we assess the influence of the nesting strategy on the model's ability to reproduce the characteristics of this severe convective event.

The initial and boundary conditions for the HARMONIE-AROME simulations were obtained from the ECMWF Integrated Forecasting System (IFS) analysis, which has a horizontal resolution of 18 km and

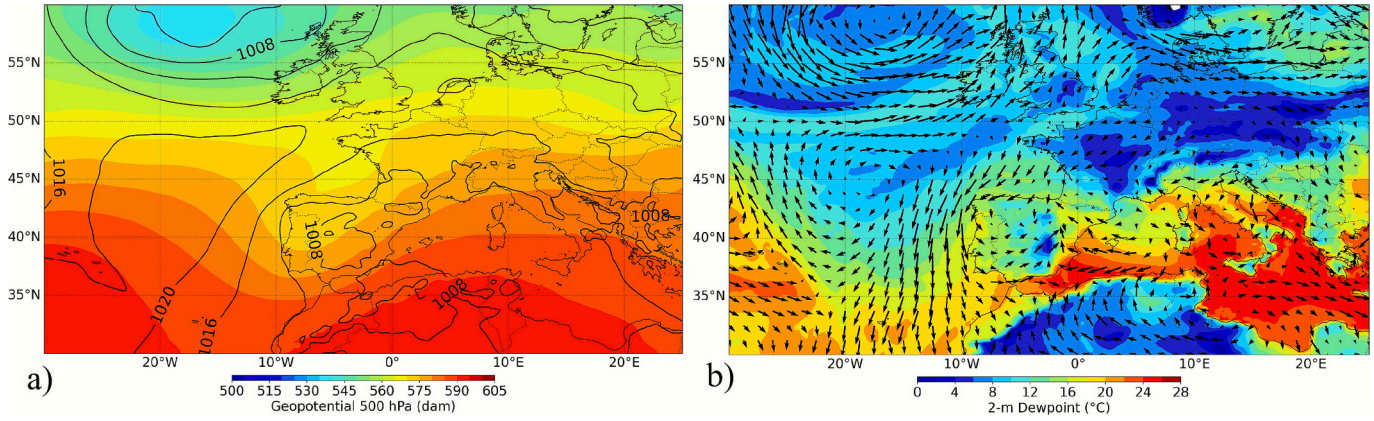

Fig. 2. On July 31, 2015, at 12:00 UTC from ERA5: a) 500 hPa geopotential height (shaded; dam) and mean sea level pressure (black contours, hPa). b) 2-m dewpoint (shaded, °C) and 10-m wind arrows.

137 vertical model levels every 6 h. Both simulations included 6 h spin-up period and covered 24 h, using 65 hybrid sigma-pressure levels and an hourly output frequency. HARMONIE-AROME is a convection-permitting model that uses a non-hydrostatic spectral dynamical core with semi-Lagrangian and semi-implicit discretization schemes. Within the HIRLAM community, extensive meteorological quality assurance is carried out before releasing the so-called reference version of the model. The objective of this reference version is to facilitate the use of the different model cycles in operational environments across the ten National Meteorological Services (NMSs) that form the HIRLAM consortium. Each reference version is validated over various domains, climates, and seasons, including both deterministic and ensemble (EPS) simulations. The reference setup for CY46 has been used in this work.

While research-oriented models such as WRF are designed for flexibility and experimentation, HARMONIE-AROME is primarily intended for operational use thus the research elasticity options are limited. Consequently, this study adopts the default operational physical parameterization settings described by Bengtsson et al. (2017). The configuration includes the Morcrette shortwave radiation scheme (Bengtsson et al., 2017; Seity et al., 2011) and the Rapid Radiative Transfer Model (RRTM) for longwave radiation scheme of (Mlawer et al., 1997). For microphysics, the version used in this study (cycle 46 h1) applies the ICE3 scheme (Lascaux et al., 2006; Pinty and Jabouille, 1998), complemented by the OCND2 option to improve winter simulations under stable boundary layer conditions over Northern Europe (Gleeson et al., 2024). As a convection-permitting system, HARMONIE-AROME does not parameterize deep convection, while shallow convection is represented through the EDMF scheme (Bengtsson et al., 2017; De Rooy et al., 2022). Turbulence is parametrized using the HARATU scheme (Bengtsson et al., 2017; De Rooy et al., 2022; Lenderink and Holtslag, 2004), and the surface processes of the Earth are modeled with SURFEXv8.1 (Le Moigne, 2018). These parameterization schemes are thoroughly documented in Gleeson et al. (2024) and have been operationally validated by the HIRLAM consortium. Finally, the HARMONIE-AROME model computes diagnostic radar reflectivity from the hydrometeor mixing ratios of the ICE-3 scheme (rain, snow, and graupel) following the formulation of Caumont et al. (2010). The computation uses the mixing ratios of rain, snow, and graupel from the ICE-3 microphysics scheme (Lascaux et al., 2006; Pinty and Jabouille, 1998). The equivalent radar reflectivity factor Ze ($mm^6\ m^{-3}$) is derived assuming Marshall–Palmer particle size distributions for each hydrometeor species. For a given hydrometeor category x, Ze is computed as:

$$Z_e = \sum_x \int_0^\infty N_x(D) D^6 dD \tag{1}$$

where $N_x(D)$is the particle size distribution following the Marshall–Palmer distribution (Marshall and Palmer, 1948), D^6 is the sixth power of particle diameter, which arises from the Rayleigh scattering approximation and dD indicates integration with respect to particle diameter. Ze ($mm^6\ m^{-3}$) is then converted to dBZ:

$$dBZ = 10log10(Ze) \tag{2}$$

Since ICE-3 does not include a prognostic hail category, simulated reflectivities tend to be underestimated in convective cores. However, this affects both experiments, as the same configuration is applied to the H500 and H500_NESTED experiments for consistency and comparability.

2.3. Observational data

The OPERA data hub (www.eumetnet.eu/opera), managed by the European Meteorological Services Network (EUMETNET), centrally collects radar volumetric raw data (ODIM_H5 format) from over 200 radars across EUMETNET member countries (Huuskonen et al., 2014). It produces three composite products (rain rate, maximum reflectivity, and one-hour rainfall accumulation) every 15 min with a 2 km horizontal resolution (Saltikoff et al., 2019). In accordance with OPERA guidelines (Huuskonen et al., 2014; Saltikoff et al., 2019), the observed reflectivity was subjected to standard quality control procedures. These procedures included the removal of ground clutter and anomalous propagation, attenuation correction (ZPHI method), and calibration checks. In addition to the OPERA data, a set of available precipitation and surface temperature observations from 236 weather stations operated by the Spanish Meteorological Agency (AEMET; Fig. 1b), covering the period from 10:00 to 20:00 UTC during the event is included to further validate both simulations. For each weather station and time step, the corresponding model output was extracted at the nearest grid point, ensuring a one-to-one comparison between simulated and observed values.

In this study, the instantaneous maximum reflectivity from OPERA and temperature and precipitation observations from weather stations are used to compare and validate these variables in H500 and H500_NESTED simulations. The temporal and spatial averages for Bias (simulated data minus observed ones), Root-Mean-Square Error (RMSE) and Linear product-moment correlation coefficient of Pearson are computed. The non-parametric Mann–Whitney *U* test (Mann and Whitney, 1947) is applied over these variables to statistically evaluate the significant differences (*p*-value) between both simulations. Moreover, temperature and precipitation Probability Density Functions (PDFs) from weather stations and both HARMONIE-AROME are computed. The PDFs represent the aggregated distribution of these paired values across all stations and time steps, rather than a single point or a single model level. This approach provides a comprehensive view of the model's performance across the entire observational network. The 12:00 UTC Murcia radiosonde is selected as a representative sounding to analyze the pre-convective environment of this severe weather event. One of the six supercells tracked within 50 km north of Murcia produced hailstones up to 8 cm in diameter. Radiosonde data are obtained from http://rawinsonde.com/ (Taszarek et al., 2021). Kinematic and thermodynamic conditions are evaluated using key parameters widely used in forecasting deep moist convection and supercells (Bunkers et al., 2000; Calvo-Sancho et al., 2022; Craven et al., 2002; Pilguj et al., 2019; Taszarek et al., 2017). These include Most-Unstable (MU), Surface-Based (SB) and Mixed-Layer averaged over 0–500 m above ground level (ML) for CAPE and Convective Inhibition (CIN). The ML Lifting Condensation Level (LCL), Level of Free Convection (LFC), deep-layer bulk Wind Shear (0–6 km, WS06), Storm-Relative Helicity (0–3 km, SRH03) are also calculated. Finally, Supercell Convective Parameter (SCP) focuses on CAPE, wind shear and SRH is also considered (Gropp and Davenport, 2018; Thompson et al., 2003). All of these parameters are compared with simulated soundings from H500_NESTED and H500 to assess their ability to reproduce the observed supercell environment.

3. Results and discussion

The H500 and H500_NESTED simulations are compared and verified against observations to address the main objective. Before validating and comparing both simulations, it is important to highlight the computational requirements of each approach. The H500_NESTED simulation involves two sequential runs: an initial simulation at 2.5 km horizontal resolution, which provides boundary and initial conditions for a subsequent 500 m resolution simulation. In contrast, the H500 simulation is performed using a single 500 m resolution domain, eliminating the need for nesting.

Due to this setup, H500_NESTED requires 250,406 System Billing Units (SBU) on the ECMWF's HPCF and takes 17 h and 51 min to complete. In comparison, H500 demands 175,106 SBU —30% less than H500_NESTED— and has a shorter runtime of 14 h and 29 min, because the H500_NESTED involves two sequential simulations (parent and nested domains), whereas H500 uses a single simulation (single-domain) approach. Although the absolute performance may vary across

HPCF systems, compilers, and parallelization strategies, the relative cost difference between single-domain and nested configurations is expected to remain, given that the latter inherently requires additional runs. Nevertheless, the magnitude of this difference could change depending on hardware architecture and job scheduling. Given this difference in computational cost at ECMWF's HPCF, the validation results must demonstrate a significant improvement in model performance to justify the added cost of the two-step one-way nesting approach.

Subsequently, the modeled maximum reflectivity is compared with radar data from the OPERA network. Although differences between H500 and H500_NESTED are minor, both exhibit some discrepancies against observations (Fig. 3). H500 shows delayed and weaker supercell

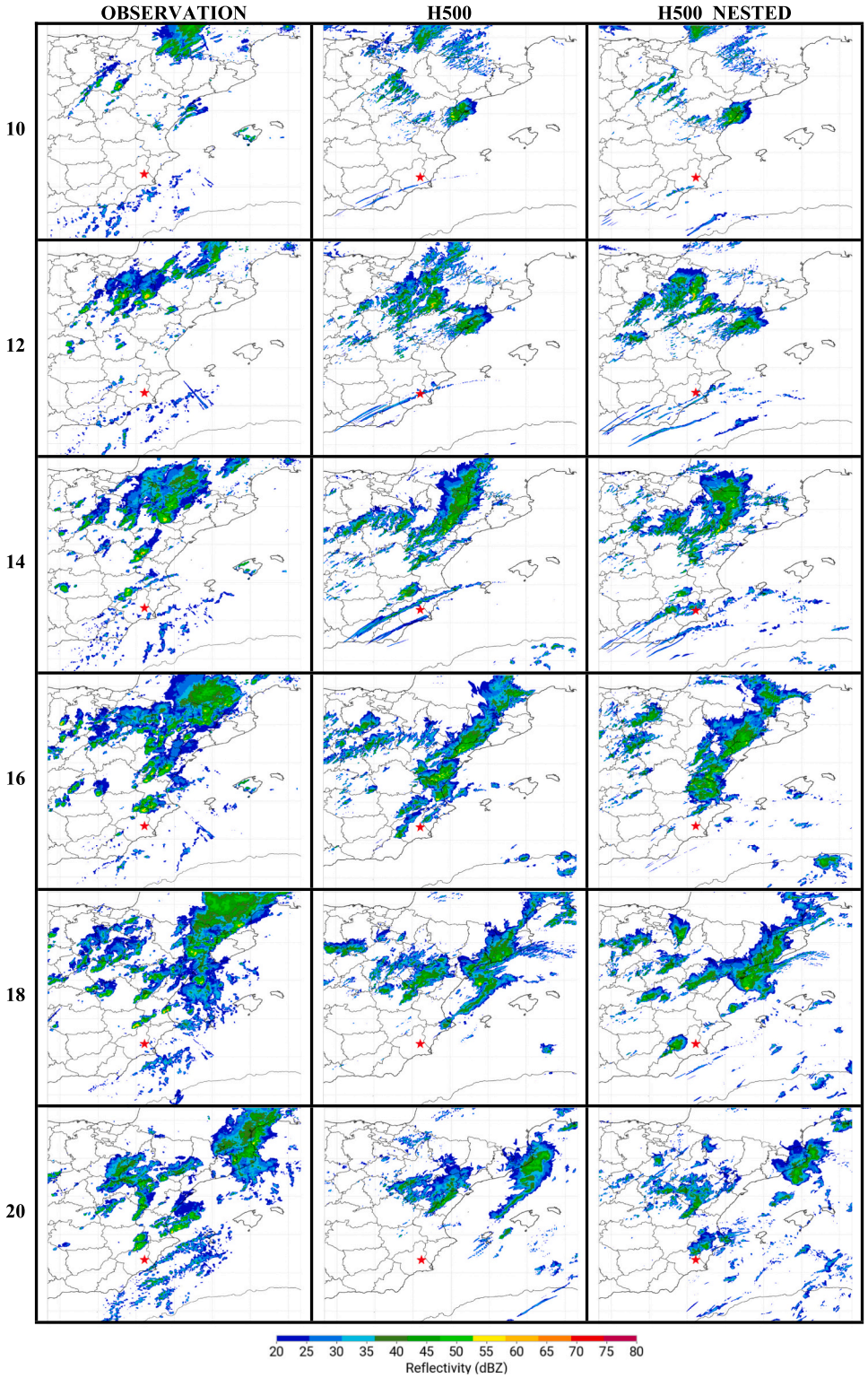

Fig. 3. Time series of maximum reflectivity (in dBZ) from OPERA (OBSERVATION) and simulated from HARMONIE-AROME configurations (H500 and H500_NESTED) between 10:00–20:00 UTC on 31 July 2015. Red star indicates the Murcia sounding station location. (For interpretation of the references to colour in this figure legend, the reader is referred to the web version of this article.)

storm development, whereas H500_NESTED better captures the supercell evolution, particularly at later stages, with improved representation of high-reflectivity cores. Analyzing the time series reveals substantial differences in the two models' ability to reproduce the observed supercells in Murcia (south of the Iberian Peninsula). At 16:00 UTC, the H500_NESTED simulation fails to reproduce the intensity and position of SP-5 (north of Murcia), whereas the H500 simulation accurately captures both its strength and location. However, between 18:00 and 20:00 UTC, the roles are reversed: H500_NESTED better captures the growth and development of SP-6. Despite this, H500_NESTED produces a spatial displacement and overestimates the supercell's intensity, while H500 fails to adequately simulate the structure and evolution of SP-6 during this period.

As expected, both simulations produce more diffuse supercell structures, lacking the fine-scale organization seen in the observation. Reflectivity is systematically underestimated, with biases of −5.85 dBZ for H500 and − 5.78 dBZ for H500_NESTED. Despite their similar RMSE values (5.45 dBZ for H500 and 5.48 dBZ for H500_NESTED) and identical correlation coefficient (0.41), H500_NESTED captures slightly higher reflectivity values and better-defined convective cores, in line with its reduced bias. Additionally, the Mann–Whitney *U* test yields a *p*-value of 0.27, indicating no statistically significant differences in reflectivity distributions between the two simulations. The underestimation of radar reflectivity may be partly attributed to the limitations of the ICE-3 microphysics scheme used in HARMONIE-AROME. ICE-3 is a single-moment scheme that does not explicitly simulate hail, a key hydrometeor in supercell cores (Lascaux et al., 2006; Pinty and Jabouille, 1998). The absence of hail and the simplified representation of graupel can lead to lower hydrometeor mixing ratios and weaker simulated radar returns. Although the nested approach improves spatial detail and intensity representation, the overall statistical performance of H500_NESTED and H500 remains similar. The nesting strategy enhances the depiction of convective structures but does not significantly improve RMSE or correlation. These findings contrast from those of Pilguj et al. (2019), who used the high-resolution WRF model to simulate an isolated tornadic supercell in Poland and reported an overestimation of maximum reflectivity in their results, using double-moment microphysics.

The PDFs for 2-m temperature and total precipitation are displayed in Fig. 4a and b, respectively. Both simulations reproduce the bimodal distribution of observed temperatures, with peaks around 19–20 °C and 27–28 °C (Fig. 4a). However, both simulations show notable discrepancies in the representation of temperature distributions. Specifically, they significantly overestimate the density of values between 15 and 20 °C and underestimate it between 20 and 25 °C. In contrast, temperatures above 25 °C are well reproduced, with H500_NESTED showing a better alignment with observations. Statistical skill scores confirm this improvement, with H500_NESTED showing a lower bias (−0.36 °C vs. -0.47 °C), lower RMSE (1.02 °C vs. 1.15 °C), and a slightly higher Pearson correlation coefficient (0.98 vs. 0.97). Additionally, a Mann–Whitney *U* test was performed to assess whether the temperature distributions from both simulations differ significantly. A 0.75 *p*-value indicates no statistically significant differences between the H500_NESTED and H500 configurations. This general temperature

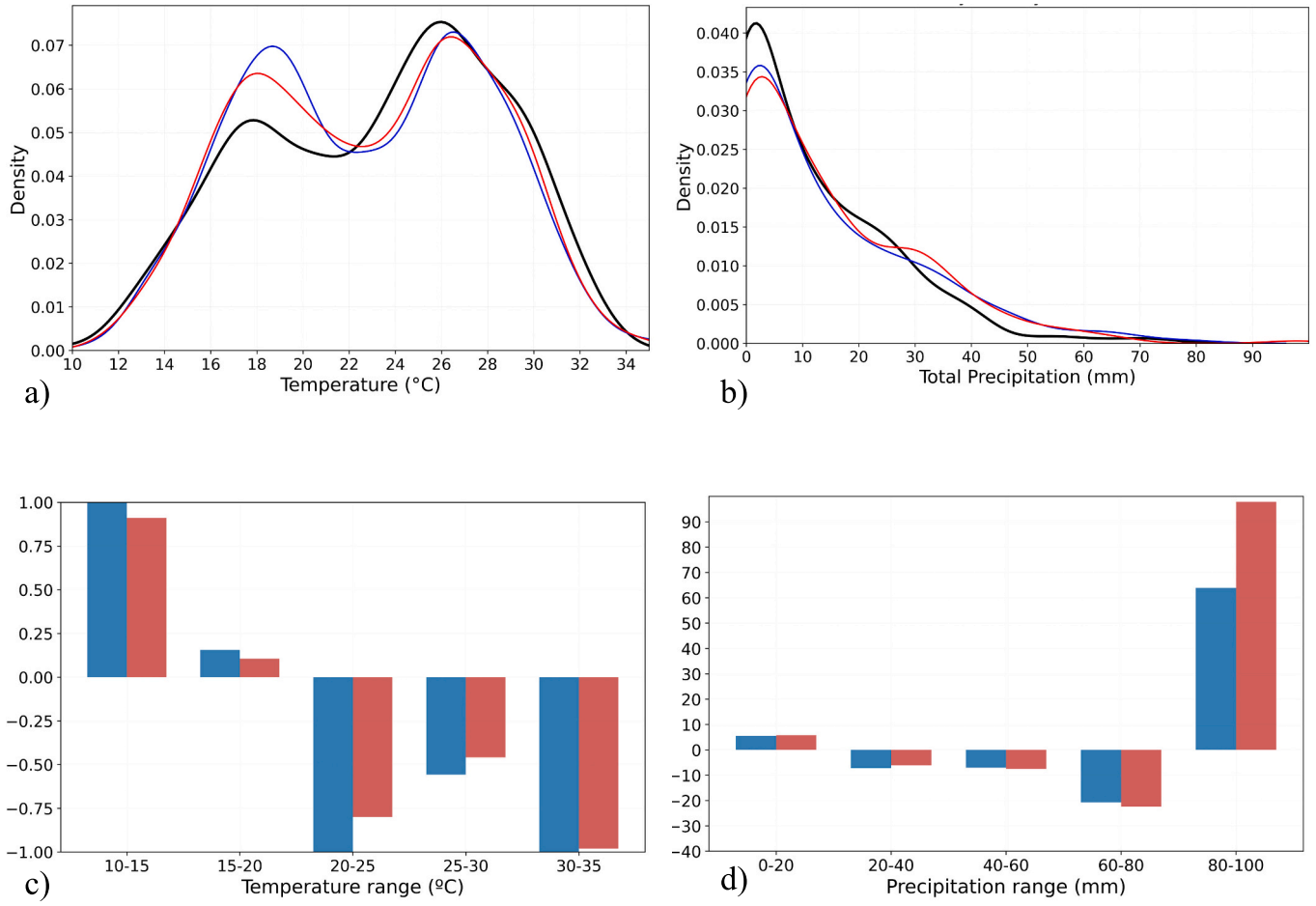

Fig. 4. Comparison of simulated and observed distributions and mean differences for two variables. PDFs for observations (black), H500_NESTED (red), and H500 (blue) for (a) 2-m temperature (°C) and (b) total precipitation (mm). Mean differences (simulation–observation) for several ranges for (c) 2-m temperature (°C) and (d) total precipitation (mm). (For interpretation of the references to colour in this figure legend, the reader is referred to the web version of this article.)

underestimation is consistent with previous high-resolution HARMONIE-AROME studies under different synoptic conditions, such as fog episodes in Tenerife-Norte airport (Fernández-González et al., 2019), showing a recurrent model behaviour rather than an isolated case. These results indicate that the nested configuration enhances the representation of temperature distribution, reducing errors and biases. Fig. 4c provides a detailed view of the mean differences between simulated and observed temperatures across different ranges. In the coolest interval (10–15 °C), both models strongly overestimate temperatures, with H500 showing a bias of +1.06 °C and H500_NESTED +0.91 °C. For the 15–20 °C range, biases become slightly positive (+0.16 °C for H500 and + 0.11 °C for H500_NESTED), indicating a small overestimation. Underestimations start in the 20–25 °C range, where H500 shows a bias of −1.06 °C and H500_NESTED of −0.80 °C. The largest negative discrepancies occur in the warmest interval (25–35 °C), with H500 at −1.24 °C and H500_NESTED at −1.00 °C. Overall, H500_NESTED consistently shows slightly smaller absolute biases than H500, but systematic underestimation persists in the mid and upper ranges after an initial overestimation at the lowest temperatures.

The overall shape of the observed total precipitation distribution is captured by H500_NESTED and H500 models (Fig. 4b), with a maximum value around 5 mm. However, both models tend to underestimate density at lower precipitation values. For higher precipitation amounts (>20 mm), both present deviations from observations, with H500_NESTED showing a slightly better fit in the distribution tail. Statistical skill scores indicate that while H500_NESTED has a higher bias (2.56 mm vs. 2.25 mm), it also achieves a slightly lower RMSE (14.17 mm vs. 14.65 mm) and a higher correlation coefficient (0.57 vs. 0.55) compared to H500. These results indicate that while both configurations successfully capture the general precipitation distribution, biases and errors persist, particularly in the representation of extreme precipitation events. Furthermore, the Mann–Whitney U test yields a p-value of 0.87, suggesting no statistically significant differences between both configurations. Harris and Durran (2010) demonstrated that two-way nesting yields improved results in simulating precipitation distributions, especially in regions with complex terrain, as it reduces errors associated with extreme precipitation. However, in this study, the differences between H500 and H500_NESTED simulations are not significant, suggesting that the advantages of two-way nesting may be less pronounced under the specific conditions analyzed here. Fig. 4d provides a detailed view of mean differences of precipitation ranges. Both configurations lightly underestimate rainfall for lowest amounts (<20 mm). Similar negative biases appear in the 20–40 mm and 41–60 mm ranges for both experiments. The largest negative discrepancies occur for 60–80 mm, with H500 at −31.9 mm and H500_NESTED at −26.3 mm. In contrast, the most extreme interval (80–100 mm) reveals substantial overestimations, particularly for H500_NESTED configuration (+97.8 mm vs. +63.9 mm for H500), indicating that nesting introduces larger errors in the extreme precipitation. These results suggest that while nesting slightly improves performance for moderate precipitation, it can significantly worsen bias for the severe precipitation, limiting its overall benefit.

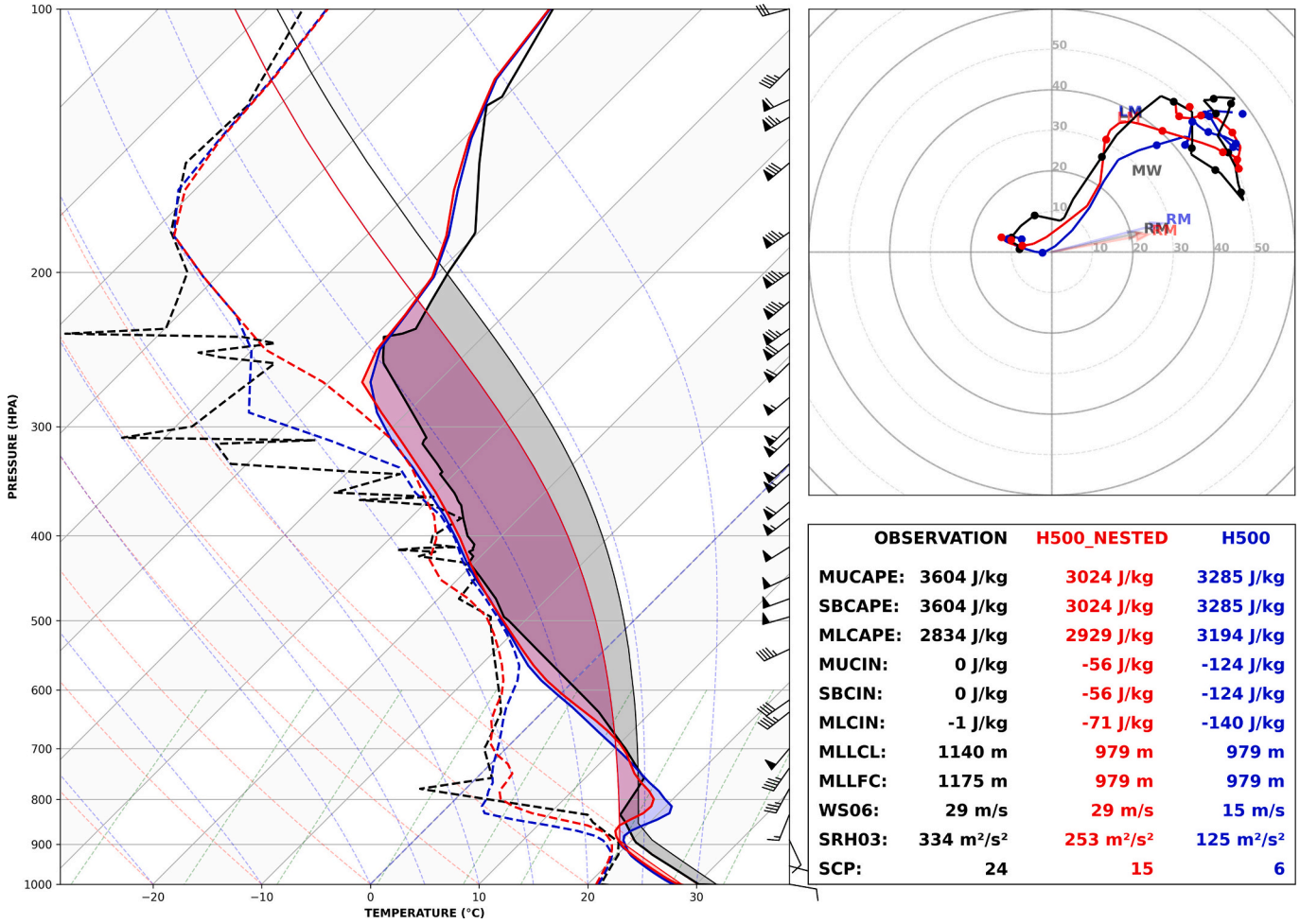

	OBSERVATION	H500_NESTED	H500
MUCAPE:	3604 J/kg	3024 J/kg	3285 J/kg
SBCAPE:	3604 J/kg	3024 J/kg	3285 J/kg
MLCAPE:	2834 J/kg	2929 J/kg	3194 J/kg
MUCIN:	0 J/kg	-56 J/kg	-124 J/kg
SBCIN:	0 J/kg	-56 J/kg	-124 J/kg
MLCIN:	-1 J/kg	-71 J/kg	-140 J/kg
MLLCL:	1140 m	979 m	979 m
MLLFC:	1175 m	979 m	979 m
WS06:	29 m/s	29 m/s	15 m/s
SRH03:	334 m²/s²	253 m²/s²	125 m²/s²
SCP:	24	15	6

Fig. 5. Skew-T log-P diagram comparing vertical profiles of temperature and dew point (in °C) and convective parameters. Observational data from the Murcia radiosonde (black) are compared with model soundings from H500_NESTED (red) and H500 (blue) at 12:00 UTC on 31 July 2015. (For interpretation of the references to colour in this figure legend, the reader is referred to the web version of this article.)

Vertical profiles observed and simulated of H500_NESTED and H500 of the supercell event at the Murcia-sounding station show a favorable environment for deep convection development (Fig. 5). Overall, both simulations capture the general trend of the observed temperature profile and the thermal inversion. However, there are significant differences in the intensity of temperature inversions and the detailed structure of the atmospheric profile. The H500_NESTED simulation achieves a closer match to the observed temperature in the lower atmospheric levels (900–800 hPa) since the inversion is more accurately captured than the H500 simulation. However, both simulations exhibit a tendency to smooth out the sharp gradients of the observed temperature inversion. In mid-levels, both simulations slightly underestimate the temperature compared to observations. The dew point has a very similar behaviour as the temperature, and the H500_NESTED has a better approximation to the observed dew point. These findings underscore the importance of incorporating higher-resolution configurations or refined physical parameterizations to better replicate the fine-scale features of atmospheric inversions, which play a critical role in modulating vertical mixing and influencing weather patterns.

Related to convective parameters, the sounding observations reveal higher MUCAPE (3604 J/kg) and SBCAPE (3604 J/kg) than the simulated ones (3024 J/kg for H500_NESTED and 3285 J/kg for H500), indicating a more unstable atmosphere profile in the observations. The lower CAPE in the simulations can be attributed to lower surface temperatures, which suggests that while the models successfully capture atmospheric instability, they tend to underestimate the potential for severe thunderstorms development. Markowski and Richardson (2010) emphasize that high MUCAPE values (> 3000 J/Kg), as seen in both observations and simulations, are strongly associated with enhanced vertical accelerations —a key factor in supercell dynamics. Consequently, an increase in MUCAPE correlates with heightened storm severity, including a greater likelihood of large hail formation (Taszarek et al., 2017; Xie et al., 2010). Therefore, the underestimation of CAPE in the simulations may lead to weaker simulated updrafts, potentially affecting the representation of supercell structure, longevity, and severity, including hail production and mesocyclone intensity. Observational sounding shows no convective inhibition (MUCIN: 0 J/kg, SBCIN: 0 J/kg), whereas the simulations introduce moderate convective inhibition, with values of −56 J/kg for H500_NESTED and − 124 J/kg for H500. This suggests a more stable atmospheric profile in the simulations, which could delay or suppress convective initiation. The discrepancy can be attributed to the lower simulated surface dew point and temperature values, which reduce the buoyancy of air parcels and increase the energy barrier required to initiate deep convection. Consequently, the simulations tend to overestimate atmospheric stability, inhibiting the development of deep convective processes. When compared to the findings of Calvo-Sancho et al. (2022), which analyzed supercell convective environments in Spain using ERA5 reanalysis, the simulated MUCAPE and MUCIN values in this event exceed the 95th percentile of ERA5 supercell hail events in northeastern Spain. This underscores the exceptional instability and inhibition present, and further suggests that even small biases in model thermodynamics can significantly impact the realism of supercell simulations and the reliability of severe weather forecasts.

The observed sounding shows a WS06 of 29 m/s, which is accurately captured by H500_NESTED. In contrast, H500 underestimates this parameter (WS06 = 15 m/s). Similarly, the observed SRH03 (334 m^2/s^2) indicates an environment highly favorable to storm rotation and organized convection, exceeding the simulated SRH03 (253 m^2/s^2) for H500_NESTED and the H500 one (125 m^2/s^2). These differences in WS06 and SRH03 are attributed to small discrepancies in the simulated wind speed and direction at low atmospheric levels compared to the observed profile (not shown), which directly impact the calculation of these parameters. The observed WS06 and SRH03 highlight a strongly favorable environment for organized convection and mesocyclone formation (Markowski and Richardson, 2010). While both simulations successfully capture the robust deep-layer shear required for supercell development, the underestimation of SRH03 in both models may result in weaker low-level rotation and an underrepresentation of tornadic potential (Thompson et al., 2003). Moreover, the observed WS06 and SRH03 values align with the higher percentiles reported in Calvo-Sancho et al. (2022), reinforcing the exceptional convective potential in the observed environment.

The hodograph reveals a curved wind profile, characteristic of significant directional and speed wind shear, which are critical components for supercell development (Rasmussen and Blanchard, 1998). The observed hodograph shows strong low-level veering associated with warm air advection and enhanced storm-relative helicity, factors that strongly enhance the potential for organized convection (Davies-Jones, 1984). While H500_NESTED and H500 simulations capture the overall hodograph structure, but discrepancies arise in wind shear, particularly in the mid-levels that may influence storm organization, as weaker wind shear can reduce mesocyclone intensity and the longevity of storm rotation (Weisman and Rotunno, 2000). Despite these discrepancies, the strong wind shear environment remains conducive to supercell development, supporting long-lived, rotating updrafts capable of producing severe weather.

The simulated MLLCL and MLLFC heights are consistent across both models (979 m), whereas the observed values a slightly higher (1140 m for MLLCL and 1175 m for MLLFC). This difference suggests a more humid and potentially less inhibited boundary layer in the observations. According to Markowski and Richardson (2010), lower MLLCL heights are associated with enhanced convective potential and an increased tornado risk in supercell environments. Furthermore, the proximity of MLLCL to MLLFC indicates a reduced threshold for convective initiation, favoring earlier storm development (Rasmussen and Blanchard, 1998). Finally, the SCP values are considerably higher in the observations (24) compared to the simulated values for H500_NESTED (15) and H500 (6). The great difference between the two SCP simulations underscores its sensitivity to the underlying model configuration. These results suggest that the simulated supercell structures may be weaker, with a diminished potential for robust supercell development and severity (Thompson et al., 2003, 2007).

Summarizing, the skill scores for the maximum reflectivity performance of H500_NESTED and H500 are comparable. Likewise, the PDFs for temperature and precipitation show only marginal differences, with both simulations closely aligned with observational distributions. Furthermore, the thermodynamic and kinematic profiles derived from the model soundings do not demonstrate substantial improvements in key parameters relevant to convective storm development, apart from the higher SCP value in H500_NESTED than H500. As a result, the higher-resolution nesting approach appears to provide limited advantages relative to the additional computational cost, requiring 30% more computational resources while offering no significant improvement over a single-domain simulation. These marginal improvements can be explained by several factors. Firstly, the parent domain at a resolution of 2.5 km already captures the main mesoscale features and synoptic forcing that strongly influenced this event, thus limiting the added value of further downscaling. Furthermore, phase errors or biases in the parent simulation are propagated into the nested domain through the one-way nesting approach, which constrains its ability to correct large-scale discrepancies. Finally, as both configurations use the same physical parameterizations, differences primarily arise from resolution rather than physics.

4. Summary and conclusions

The six supercell events that formed in the complex orography of eastern Iberian Peninsula on July 31, 2015, are simulated using two HARMONIE-AROME nesting strategies to evaluate their performance. The first, H500_NESTED, employs a two-step nesting approach, while the second, H500, uses a single-domain setup, with both final spatial

resolutions of 500 m. The ability of both nesting approaches is evaluated by comparing maximum reflectivity observations from OPERA radar and precipitation and temperature from weather stations. The pre-convective conditions are validated using the Murcia radiosonde.

The main conclusions are as follows:

- **Computational efficiency:** On the ECMWF's HPCF, H500_NESTED require approximately 30% more computational resources than H500 because it involves two sequential simulations (parent and nested domains), whereas H500 uses a single-domain configuration. Given that this study is conducted exclusively within the ECMWF HPCF, the recommendation should be interpreted with caution.
- **Model performance:** Both H500_NESTED and H500 reproduce the overall structure of the supercell outbreak. H500_NESTED provides slightly better representation of convective core structure, high reflectivity values, and a closer approximation to observed temperature and wind profiles. However, precipitation results show a mixed performance: while H500_NESTED slightly reduces bias for moderate rainfall, it introduces larger errors in the most extreme range, where overestimation in the nested experiment is significantly greater than in H500. Both configurations systematically underestimate light precipitation and overestimate moderate to heavy amounts, but the nested approach does not consistently improve accuracy and, in some cases, worsens performance for extreme rainfall. Although these findings indicate that the benefits of nesting are limited and less consistent for precipitation than for temperature (where improvements are more evident), the gain is minimal when considered in relation to the increased computational cost.
- **Environmental conditions:** Both simulations capture the general atmospheric profile but tend to underestimate instability and helicity, which may affect the accurate prediction of storm intensity and rotation. Convective parameters such as CIN, WS06, SRH03, and SCP in H500_NESTED are closer to those observed in the Murcia sounding, while CAPE values in H500 match observations more closely. These results confirm that the environment is highly favorable for deep convection, as indicate by CAPE (3604 J/kg), SRH03 (334 m^2/s^2), and WS06 (29 m/s).
- **Implications and limitations:** This study is motivated by the need to improve the understanding and prediction of severe convective storms in complex terrain, and the scarce bibliography available on nesting results with HARMONIE-AROME simulations. The results highlight both the benefits and limitations of high-resolution nested configurations for representing mesoscale and convective-scale processes. While nesting improves temperature representation and slightly reduces bias for moderate precipitation, its overall impact on precipitation skill scores is inconsistent and, in the most extreme ranges, may even worsen performance. Although this analysis is based on a single, well-documented event, it serves as a proof of concept and provides a framework for future multi-event and seasonal assessments to validate the robustness and cost-effectiveness of the nesting strategy.
- **Future work:** Future research will extend this analysis to multiple cases, incorporate advanced data assimilation techniques (e.g., radar and satellite observations), and test alternative physical parameterizations to further enhance forecast skill. Given the negligible advantages of the nesting approach in this study, future simulations may prioritize single-domain high-resolution setups like H500 for severe convective event analysis, particularly when computational resources are limited. Also, it would be interesting to investigate the influence of complex orography and a warmer Mediterranean Sea in the development of these severe convective events.

CRediT authorship contribution statement

J. Díaz-Fernández: Methodology, Software, Validation, Writing – review & editing, Data curation, Formal analysis. **C. Calvo-Sancho:** Methodology, Software, Validation, Data curation, Formal analysis. **M. López-Reyes:** Writing – review & editing, Supervision. **P. Bolgiani:** Methodology, Software, Validation, Writing – review & editing. **J.J. González-Alemán:** Methodology, Supervision, Investigation. **A. Morata:** Methodology, Data curation. **D. Santos-Muñoz:** Methodology, Software. **M.L. Martín:** Methodology, Validation, Writing – review & editing, Supervision, Funding acquisition, Resources, Investigation.

Declaration of competing interest

The authors declare that there are no conflicts of interest regarding the publication of this paper.

Data availability

Data will be made available on request.

Acknowledgments

This research belongs to PID2023-146344OB-I00 (CONSCIENCE) supported by the Ministerio de Ciencia, Innovación y Universidades (MICIU), AEI/10.13039/501100011033/FEDER and UE and the ECMWF Special Projects (SPESMART and SPESVALE).

References

Avolio, E., Miglietta, M.M., 2021. Multiple tornadoes in the Italian Ionian regions: Observations, sensitivity tests and mesoscale analysis of convective storm environmental parameters. Atmos. Res. 263. https://doi.org/10.1016/j.atmosres.2021.105800.

Bengtsson, L., Andrae, U., Aspelien, T., Batrak, Y., Calvo, J., de Rooy, W., Gleeson, E., Hansen-Sass, B., Homleid, M., Hortal, M., Ivarsson, K.I., Lenderink, G., Niemelä, S., Nielsen, K.P., Onvlee, J., Rontu, L., Samuelsson, P., Muñoz, D.S., Subias, A., Køltzow, M.Ø., 2017. The HARMONIE-AROME model configuration in the ALADIN-HIRLAM NWP system. Mon. Weather Rev. 145 (5), 1919–1935. https://doi.org/10.1175/MWR-D-16-0417.1.

Bližňák, V., Sokol, Z., Zacharov, P., 2017. Nowcasting of deep convective clouds and heavy precipitation: comparison study between NWP model simulation and extrapolation. Atmos. Res. 184, 24–34. https://doi.org/10.1016/j.atmosres.2016.10.003.

Browning, K.A., 1962. Cellular structure of convective storms. In: The Meteorological Magazine, 91, issue 1058.

Bunkers, M.J., Klimowski, B.A., Zeitler, J.W., Thompson, R.L., Weisman, M.L., 2000. Predicting supercell motion using a new hodograph technique. Weather Forecast. 15 (1). https://doi.org/10.1175/1520-0434(2000)015<0061:PSMUAN>2.0.CO;2.

Calvo-Sancho, C., Martín, Y., 2021. Supercell Pre-convective Environments in Spain: a dynamic downscaling of ERA-5. Reanalysis 5194.

Calvo-Sancho, C., Díaz-Fernández, J., Martín, Y., Bolgiani, P., Sastre, M., González-Alemán, J.J., Santos-Muñoz, D., Farrán, J.I., Martín, M.L., 2022. Supercell convective environments in Spain based on ERA5: hail and non-hail differences. Weather Climate Dyn. 3 (3), 1021–1036. https://doi.org/10.5194/wcd-3-1021-2022.

Calvo-Sancho, C., Bolgiani, P., Subias, Á., Sastre, M., González-Alemán, J.J., Martín, M. L., 2023a. Horizontal kinetic energy analysis of tropical transition simulations with the WRF and HARMONIE-AROME models. Q. J. Roy. Meteorol. Soc. 149 (756). https://doi.org/10.1002/qj.4523.

Calvo-Sancho, C., Quitián-Hernández, L., Bolgiani, P., González-Alemán, J.J., Santos-Muñoz, D., Martín, M.L., 2023b. Assessment of HARMONIE-AROME in the simulation of the convective activity associated to a subtropical transition using satellite data. Atmospheric Res. 290. https://doi.org/10.1016/j.atmosres.2023.106794.

Castro, A., Sánchez, J.L., Fraile, R., 1992. Statistical comparison of the properties of thunderstorms in different areas around the Ebro-Valley (Spain). Atmos. Res. 28 (3–4), 237–257. https://doi.org/10.1016/0169-8095(92)90011-X.

Caumont, O., Ducrocq, V., Wattrelot, Ér, Jaubert, G.Èv., Pradier-Vabre, S., 2010. 1D+3DVar assimilation of radar reflectivity data: a proof of concept. Tellus Ser. A Dyn. Meteorol. Oceanogr. 62 (2). https://doi.org/10.1111/j.1600-0870.2009.00430.x.

Craven, J.P., Jewell, R.E., Brooks, H.E., 2002. Comparison between observed convective cloud-base heights and lifting condensation level for two different lifted parcels. Weather Forecast. 17 (4). https://doi.org/10.1175/1520-0434(2002)017<0885:CBOCCB>2.0.CO;2.

Dahl, J.M.L., 2006. Supercells - Their Dynamics and Prediction, p. 122.

Davies, J.M., Johns, R.H., 2011. Some wind and instability parameters associated with strong and violent tornadoes: 1. Wind Shear Helicity. https://doi.org/10.1029/gm079p0573.

Davies-Jones, R., 1984. STREAMWISE vorticity: the origin of updraft rotation in supercell storms. J. Atmos. Sci. 41 (20). https://doi.org/10.1175/1520-0469(1984)041<2991:SVTOOU>2.0.CO;2.

De Elía, R., Laprise, R., Denis, B., 2002. Forecasting skill limits of nested, limited-area models: a perfect-model approach. Mon. Weather Rev. 130 (8). https://doi.org/10.1175/1520-0493(2002)130<2006:fslonl>2.0.co;2.

De Martin, F., Davolio, S., Miglietta, M.M., Levizzani, V., 2024. A conceptual model for the development of tornadoes in the complex orography of the po valley. Mon. Weather Rev. 152 (6). https://doi.org/10.1175/MWR-D-23-0222.1.

De Martin, F., Pavan, F., Carlon, N., Cioni, G., Rozoff, C., Poli, V., Carpentari, S., Miglietta, M.M., 2025. A significant tornado event near a dryline bulge in Northern Italy. Weather Forecast. 40 (11). https://doi.org/10.1175/WAF-D-25-0071.1.

De Rooy, W.C., Siebesma, P., Baas, P., Lenderink, G., De Roode, S.R., De Vries, H., Van Meijgaard, E., Meirink, J.F., Tijm, S., Van't Veen, B., 2022. Model development in practice: a comprehensive update to the boundary layer schemes in HARMONIE-AROME cycle 40. Geosci. Model Dev. 15 (4). https://doi.org/10.5194/gmd-15-1513-2022.

Duda, J.D., Gallus, W.A., 2010. Spring and summer midwestern severe weather reports in supercells compared to other morphologies. Weather Forecast. 25 (1). https://doi.org/10.1175/2009WAF2222338.1.

Farnell Barqué, C., Rigo, T., Martin-Vide, J., Úbeda, X., 2024. Internal structure of giant hail in a catastrophic event in Catalonia (NE Iberian Peninsula). Front. Environ. Sci. 12 (1479824).

Fernández-González, S., Bolgiani, P., Fernández-Villares, J., González, P., García-Gil, A., Suárez, J.C., Merino, A., 2019. Forecasting of poor visibility episodes in the vicinity of Tenerife Norte Airport. Atmos. Res. 223 (February), 49–59. https://doi.org/10.1016/j.atmosres.2019.03.012.

Font, Inocencio, 2000. Climatología de España y Portugal. In: Ediciones Universidad de Salamanca.

García-Ortega, E., Hermida, L., Hierro, R., Merino, A., Gascón, E., Fernández-González, S., Sánchez, J.L., López, L., 2014. Anomalies, trends and variability in atmospheric fields related to hailstorms in North-Eastern Spain. Int. J. Climatol. 34 (11). https://doi.org/10.1002/joc.3910.

Gascón, E., Merino, A., Sánchez, J.L., Fernández-González, S., García-Ortega, E., López, L., Hermida, L., 2015. Spatial distribution of thermodynamic conditions of severe storms in southwestern Europe. Atmos. Res. 164–165, 194–209. https://doi.org/10.1016/j.atmosres.2015.05.012.

Giorgi, F., Mearns, L.O., 1999. Introduction to special section: Regional climate modeling revisited. J. Geophys. Res. Atmos. 104 (D6). https://doi.org/10.1029/98JD02072.

Gleeson, E., Kurzeneva, E., De Rooy, W., Rontu, L., Martín Pérez, D., Clancy, C., Ivarsson, K.-I., Engdahl, B.J., Tijm, S., Nielsen, K.P., 2024. The cycle 46 configuration of the harmonie-arome forecast model. Meteorology 3 (4), 354–390.

Gropp, M.E., Davenport, C.E., 2018. The impact of the nocturnal transition on the lifetime and evolution of supercell thunderstorms in the great plains. Weather Forecast. 33 (4), 1045–1061. https://doi.org/10.1175/WAF-D-17-0150.1.

Harris, L.M., Durran, D.R., 2010. An idealized comparison of one-way and two-way grid nesting. Mon. Weather Rev. 138 (6). https://doi.org/10.1175/2010MWR3080.1.

Homar, V., Gayà, M., Romero, R., Ramis, C., Alonso, S., 2003. Tornadoes over complex terrain: an analysis of the 28th August 1999 tornadic event in eastern Spain. Atmos. Res. 67–68 (August 1999), 301–317. https://doi.org/10.1016/S0169-8095(03)00064-4.

Huuskonen, A., Saltikoff, E., Holleman, I., 2014. The operational weather radar network in Europe. Bull. Am. Meteorol. Soc. 95 (6). https://doi.org/10.1175/BAMS-D-12-00216.1.

Kaltenböck, R., Diendorfer, G., Dotzek, N., 2009. Evaluation of thunderstorm indices from ECMWF analyses, lightning data and severe storm reports. Atmos. Res. 93 (1–3). https://doi.org/10.1016/j.atmosres.2008.11.005.

Kotroni, V., Lagouvardos, K., 2016. Lightning in the Mediterranean and its relation with sea-surface temperature. Environ. Res. Lett. 11 (3). https://doi.org/10.1088/1748-9326/11/3/034006.

Kunz, M., Wandel, J., Fluck, E., Baumstark, S., Mohr, S., Schemm, S., 2020. Ambient conditions prevailing during hail events in Central Europe. Nat. Hazards Earth Syst. Sci. 20 (6). https://doi.org/10.5194/nhess-20-1867-2020.

Lascaux, F., Richard, E., Pinty, J.P., 2006. Numerical simulations of three different MAP IOPs and the associated microphysical processes. Q. J. Roy. Meteorol. Soc. 132 (619). https://doi.org/10.1256/qj.05.197.

Le Moigne, P., 2018. SURFEX Scientific Documentation, V8, p. 1.

Lenderink, G., Holtslag, A.A.M., 2004. An updated length-scale formulation for turbulent mixing in clear and cloudy boundary layers. Q. J. Roy. Meteorol. Soc. 130 C (604). https://doi.org/10.1256/qj.03.117.

Mann, H.B., Whitney, D.R., 1947. On a Test of whether one of two Random Variables is Stochastically Larger than the other. Ann. Math. Stat. 18 (1). https://doi.org/10.1214/aoms/1177730491.

Markowski, P., Richardson, Y., 2010. Mesoscale meteorology in midlatitudes. Mesoscale Meteorol. Midlatitudes. https://doi.org/10.1002/9780470682104.

Markowski, P.M., Dotzek, N., 2011. A numerical study of the effects of orography on supercells. Atmos. Res. 100 (4). https://doi.org/10.1016/j.atmosres.2010.12.027.

Marshall, J.S., Palmer, W.M.K., 1948. The distribution of raindrops with size. J. Meteorol. 5 (4). https://doi.org/10.1175/1520-0469(1948)005<0165:tdorws>2.0.co;2.

Martín, Y., Cívica, M., Pham, E., 2021. Constructing a supercell database in spain using publicly available two-dimensional radar images and citizen science. Ann. Am. Assoc. Geogr. 111 (5), 1346–1366. https://doi.org/10.1080/24694452.2020.1812371.

Merino, A., García-Ortega, E., López, L., Sánchez, J.L., Guerrero-Higueras, A.M., 2013. Synoptic environment, mesoscale configurations and forecast parameters for hailstorms in Southwestern Europe. Atmos. Res. 122, 183–198. https://doi.org/10.1016/j.atmosres.2012.10.021.

Miglietta, M.M., Mazon, J., Rotunno, R., 2017. Numerical simulations of a tornadic supercell over the mediterranean. Weather Forecast. 32 (3). https://doi.org/10.1175/WAF-D-16-0223.1.

Mlawer, E.J., Taubman, S.J., Brown, P.D., Iacono, M.J., Clough, S.A., 1997. Radiative transfer for inhomogeneous atmospheres: RRTM, a validated correlated-k model for the longwave. J. Geophys. Res. Atmos. 102 (14). https://doi.org/10.1029/97jd00237.

Mora, M., Riesco, J., De Pablo Dávila, F., Rivas Soriano, L., 2015. Atmospheric background associated with severe lightning thunderstorms in Central Spain. Int. J. Climatol. 35 (4), 558–569. https://doi.org/10.1002/joc.4002.

Nisi, L., Martius, O., Hering, A., Kunz, M., Germann, U., 2016. Spatial and temporal distribution of hailstorms in the Alpine region: a long-term, high resolution, radar-based analysis. Q. J. Roy. Meteorol. Soc. 142 (697). https://doi.org/10.1002/qj.2771.

Park, S., Berenguer, M., Sempere-Torres, D., 2019. Long-term analysis of gauge-adjusted radar rainfall accumulations at European scale. J. Hydrol. 573. https://doi.org/10.1016/j.jhydrol.2019.03.093.

Pilguj, N., Taszarek, M., Pajurek, Ł., Kryza, M., 2019. High-resolution simulation of an isolated tornadic supercell in Poland on 20 June 2016. Atmos. Res. 218, 145–159. https://doi.org/10.1016/j.atmosres.2018.11.017.

Pinty, J.P., Jabouille, P., 1998. A mixed-phase cloud parameterization for use in mesoscale non-hydrostatic model: simulations of a squall line and of orographic precipitations. On Cloud Phys. 217–220.

Púčik, T., Groenemeijer, P., Rýva, D., Kolář, M., 2015. Proximity soundings of severe and nonsevere thunderstorms in Central Europe. Mon. Weather Rev. 143 (12), 4805–4821. https://doi.org/10.1175/MWR-D-15-0104.1.

Púcik, T., Castellano, C., Groenemeijer, P., Kühne, T., Rädler, A.T., Antonescu, B., Faust, E., 2019. Large hail incidence and its economic and societal impacts across Europe. Mon. Weather Rev. 147 (11). https://doi.org/10.1175/MWR-D-19-0204.1.

Quirantes Calvo, J.A., Riesco Martín, J., Núñez Mora, J.Á., 2014. Características básicas de las supercélulas en España. Características Básicas de Las Supercélulas En España 1–57. https://doi.org/10.31978/281-14-008-x.

Quitián-Hernández, L., Bolgiani, P., Santos-Muñoz, D., Sastre, M., Díaz-Fernández, J., González-Alemán, J.J., Farrán, J.I., Lopez, L., Valero, F., Martín, M.L., 2021. Analysis of the October 2014 subtropical cyclone using the WRF and the HARMONIE-AROME numerical models: Assessment against observations. Atmos. Res. 260. https://doi.org/10.1016/j.atmosres.2021.105697.

Rasmussen, E.N., Blanchard, D.O., 1998. A baseline climatology of sounding-derived supercell and tornado forecast parameters. Weather Forecast. 13 (4), 1148–1164. https://doi.org/10.1175/1520-0434(1998)013<1148:ABCOSD>2.0.CO;2.

Rigo, T., Rodríguez, O., Bech, J., Farnell, C., 2022. An observational analysis of two companion supercell storms over complex terrain. Atmos. Res. 272 (August 2021), 106149. https://doi.org/10.1016/j.atmosres.2022.106149.

Rodríguez, O., Bech, J., 2021. Tornadic environments in the Iberian Peninsula and the Balearic Islands based on ERA5 reanalysis. Int. J. Climatol. 41 (S1), E1959–E1979. https://doi.org/10.1002/joc.6825.

Romero, R., Doswell, C.A., Ramis, C., 2000. Mesoscale numerical study of two cases of long-lived quasi-stationary convective systems over eastern Spain. Mon. Weather Rev. 128 (11). https://doi.org/10.1175/1520-0493(2001)129<3731:MNSOTC>2.0.CO;2.

Rotunno, R., Klemp, J.B., 1982. The influence of shear-induced pressure gradient on thunderstorm motion. Mon. Weather Rev. 110 (2). https://doi.org/10.1175/1520-0493(1982)110<0136:TIOTSI>2.0.CO;2.

Saltikoff, E., Haase, G., Delobbe, L., Gaussiat, N., Martet, M., Idziorek, D., Leijnse, H., Novák, P., Lukach, M., Stephan, K., 2019. OPERA the radar project. Atmosphere 10 (6). https://doi.org/10.3390/atmos10060320.

Seity, Y., Brousseau, P., Malardel, S., Hello, G., Bénard, P., Bouttier, F., Masson, V., 2011. The AROME-France convective-scale operational model. Monthly Weather Review 139 (3), 976–991.

Skamarock, W.C., Klemp, J.B., Dudhia, J.B., Gill, D.O., Barker, D.M., Duda, M.G., Huang, X.-Y., Wang, W., Powers, J.G., 2021. A Description of the Advanced Research WRF Model Version 4.3. NCAR Technical Note, TN–556+STR(July).

Taszarek, M., 2020. Severe convective storms across Europe and the United States. Part II: ERA5 environments associated with lightning, large hail, severe wind, and tornadoes. J. Climate 33 (24), 10437–10453. https://doi.org/10.1175/JCLI-D-20-0346.1.

Taszarek, M., Brooks, H.E., Czernecki, B., 2017. Sounding-derived parameters associated with convective hazards in Europe. Mon. Weather Rev. 145 (4), 1511–1528. https://doi.org/10.1175/MWR-D-16-0384.1.

Taszarek, M., Brooks, H.E., Czernecki, B., Szuster, P., Fortuniak, K., 2018. Climatological aspects of convective parameters over Europe: a comparison of ERA-interim and sounding data. J. Climate 31 (11), 4281–4308. https://doi.org/10.1175/JCLI-D-17-0596.1.

Taszarek, M., Allen, J., Púčik, T., Groenemeijer, P., Czernecki, B., Kolendowicz, L., Lagouvardos, K., Kotroni, V., Schulz, W., 2019. A climatology of thunderstorms across Europe from a synthesis of multiple data sources. J. Climate 32 (6), 1813–1837. https://doi.org/10.1175/JCLI-D-18-0372.1.

Taszarek, M., Pilguj, N., Allen, J.T., Gensini, V., Brooks, H.E., Szuster, P., 2021. Comparison of convective parameters derived from ERA5 and MERRA-2 with rawinsonde data over Europe and North America. Journal of Climate 34 (8), 3211–3237.

Thompson, R.L., Edwards, R., Hart, J.A., Elmore, K.L., Markowski, P., 2003. Close proximity soundings within supercell environments obtained from the rapid update cycle. Weather Forecast. 18 (6). https://doi.org/10.1175/1520-0434(2003)018<1243:CPSWSE>2.0.CO;2.

Thompson, R.L., Mead, C.M., Edwards, R., 2007. Effective storm-relative helicity and bulk shear in supercell thunderstorm environments. Weather Forecast. 22 (1), 102–115. https://doi.org/10.1175/WAF969.1.

Tiesi, A., Mazzà, S., Conte, D., Ricchi, A., Baldini, L., Montopoli, M., Picciotti, E., Vulpiani, G., Ferretti, R., Miglietta, M.M., 2022. Numerical simulation of a giant-hail-bearing mediterranean supercell in the Adriatic Sea. Atmosphere 13 (8). https://doi.org/10.3390/atmos13081219.

Trefalt, S., Martynov, A., Barras, H., Besic, N., Hering, A.M., Lenggenhager, S., Noti, P., Röthlisberger, M., Schemm, S., Germann, U., Martius, O., 2018. A severe hail storm in complex topography in Switzerland - Observations and processes. Atmos. Res. 209. https://doi.org/10.1016/j.atmosres.2018.03.007.

Weisman, M.L., Rotunno, R., 2000. The use of vertical wind shear versus helicity in interpreting supercell dynamics. J. Atmos. Sci. 57 (9). https://doi.org/10.1175/1520-0469(2000)057<1452:TUOVWS>2.0.CO;2.

Westermayer, A.T., Groenemeijer, P., Pistotnik, G., Sausen, R., Faust, E., 2017. Identification of favorable environments for thunderstorms in reanalysis data. Meteorol. Z. 26 (1), 59–70. https://doi.org/10.1127/metz/2016/0754.

Xie, B., Zhang, Q., Wang, Y., 2010. Observed characteristics of hail size in four regions in China during 1980-2005. J. Climate 23 (18), 4973–4982. https://doi.org/10.1175/2010JCLI3600.1.